Minimum-cost optimization of nonlinear fluid viscous dampers and their supporting members for seismic retrofitting

Nicolò Pollini[*1], Oren Lavan[†1] and Oded Amir[‡1]

[1]Faculty of Civil and Environmental Engineering, Technion - Israel Institute of Technology, Haifa, Israel

Abstract

This paper presents an effective approach for achieving minimum-cost designs for seismic retrofitting using nonlinear fluid viscous dampers. The damping coefficients of the dampers, and the stiffness co-efficients of the supporting braces are designed by an optimization algorithm. A realistic retrofitting cost function is minimized subject to constraints on inter-story drifts at the peripheries of frame structures. The cost function accounts for costs related to both the topology and the sizes of the dampers. The behavior of each damper-brace element is defined by the Maxwell model, where the force-velocity relation of the nonlinear dampers is formulated with a fractional power law. The optimization problem is first posed and solved as a mixed-integer problem. To reduce the computational effort required in the optimization, the problem is then re-formulated with continuous variables only and solved with a gradient-based algorithm. Material interpolation techniques, that have been successfully applied in topology optimization and in multi-material optimization, play a key role in achieving practical final design solutions with a reasonable computational effort. Promising results attained for 3-D irregular frames are presented and discussed.

Keywords: Energy dissipation devices; Viscous dampers; Seismic retrofitting; Irregular structures; Topology and sizing optimization; Material interpolation functions.

1 Introduction

Fluid viscous dampers are energy dissipation systems that became very popular in earthquake engineering. They have been extensively used in several branches of the US military, and after the end of the Cold War in 1990 they became available for civil applications [1]. The history of successful applications of fluid viscous dampers in the military proved their reliability, and their use for seismic purposes was validated after proper testing between the years 1990 and 1993 [2, 3]. In this period, it was also shown that the use of fluid viscous dampers is also appropriate for wind and other types of transient excitations. The advantage of using fluid viscous dampers for seismic design and retrofitting is strongly related to their ability to dissipate part of the energy transferred from the earthquake to the structure, thus reducing the deformation demand of the structure. As a result, if properly designed, an added damping system could enhance the structural performance of new and existing buildings under seismic excitation, improving also their safety.

Viscous dampers have been tested under earthquake loading and models for predicting their behavior have been proposed [4]. These tests showed that the hysteretic behavior of fluid viscous dampers can be defined by a nonlinear fractional power law of the form:

$$f_d = c_d sgn(v_d)|v_d|^\alpha \tag{1}$$

---

[*]nicolo@campus.technion.ac.il

[†]lavan@technion.ac.il

[‡]odedamir@technion.ac.il

where f_d is the force in the damper, c_d its damping coefficient, sgn the signum function, v_d the relative velocity between the dampers' ends, and α the velocity exponent. In general, α can vary between 0.15 and 1 [5, 6]. In [7] it was also showed that nonlinear fluid viscous dampers can achieve the same response reduction in a structure of linear viscous dampers, but with smaller forces in the dampers. And since the dampers' cost depends also on their peak force, the use of dampers with a nonlinear behavior may have also economic advantages. Thus, nowadays engineers and producers consider the more general formulation for the damper's force-velocity relation based on the nonlinear fractional power law given in Eq. (1) [8, 9, 10, 11, 12, 13, 14]. In this work too, we will consider this formulation of the dampers' viscous behavior.

In general, dampers are connected to the structure and to a supporting brace, and often the assumption of "infinitely stiff" braces is made. As a matter of fact, braces have an upper limit in terms of their stiffness. Considering a finite stiffness of the brace could significantly affect the damper-brace mechanical behavior [15]. It follows that the ratio between the size of a damper and its supporting brace becomes of crucial importance. For example, an unproportionate high damping coefficient may cause the locking of a viscous damper during an earthquake, with a consequent concentration of the deformations on the brace. This would result in an undesired damper-brace behavior. From these observations comes the need for a simultaneous optimal design of the fluid viscous dampers and their supporting braces. This is reflected is several research contributions [16, 17, 18, 19, 20, 21, 22]. In particular, in [17] viscous dampers are designed through an optimization procedure considering a given ratio between the damping coefficient and the stiffness coefficient . The results show that not considering the finite stiffness of the dampers and the supporting braces would result in an overestimation of the damper's effectiveness, thus leading in some cases to not conservative results. A gradient-based approach for the simultaneous design of viscoelastic dampers and their supporting braces was presented in [18]. Also in this work it was showed that when the brace stiffness is limited, it becomes of major importance to include it in the damper-brace model. For these reasons, in this work the design of the added damping system will involve both the dampers and their supporting braces.

There are few aspects that affect the performance of an added damping system based on fluid viscous dampers. The first is the size of the dampers, which is typically expressed in terms of the peak resisting force that they can produce. Then, the distribution of the dampers within the structure that needs to be retrofitted. These aspects strongly influence the possibility of reducing effectively peak inter-story drifts and story accelerations of structures subject to seismic excitation [23, 24]. Moreover, the dampers' size and distribution have a crucial effect on the retrofitting cost, as we will see later on, and can significantly determine whether fluid viscous dampers will be preferred over other energy dissipation technologies. As a consequence, methodologies have been proposed for the optimal distribution and sizing of viscous dampers. Several authors proposed methodologies for the optimal distribution of given sets of dampers with predefined properties [25, 26, 27]. Although these are practical approaches, and they identify optimized distributions of dampers, they need to predefine many of the design aspect beforehand, such as the number of the dampers to be allocated and their sizes. Other authors focused on the more general optimization problem of the simultaneous dampers' distribution and size selection [28, 24, 29]. These approaches select the dampers' sizes from a set of predefined discrete values. As a result, they identify practical dampers' distributions, but typically with a high computational cost due to the combinatorial nature of the problem. To reduce the computational cost of the problem at hand, other methodologies have been proposed where the optimization problem is formulated with continuous design variables only. The design variables are typically the damping coefficients of the dampers characterizing their mechanical behavior [30, 31, 32, 33, 35, 36, 37, 34, 38, 39]. These methodologies based on continuous problem formulations result in optimized distributions of dampers with a wide variety of damping coefficients. To transform these design solutions into practical ones, rounding techniques or interpretation of the results should be applied. Unfortunately it is not yet clear how to transform continuous dampers distributions into practical ones, nor whether the optimality of the solutions achieved could be spoiled due to the interpretation of the results. Recently an attempt was made to develop methodologies able to identify practical distributions of dampers with a reasonable computational cost. In [40], for example, the authors propose a gradient-based optimization approach for the placement and sizing of linear viscous dampers. The dampers are selected from a limited number of available size-groups (i.e. dampers with identical damping coefficients), and distributed in irregular 3-D frames by an optimization algorithm. Moreover,

the properties of each size-group are also part of the variables of the problem. In [41] this approach is further extended considering a more complete realistic retrofitting cost function as the objective function to be minimized. The cost function includes costs associated with the dampers' distribution in the structure, the manufacturing of the dampers, and the prototype testing. However, it should be mentioned that in these optimization-based approaches, linear viscous dampers connected to infinitely stiff braces were considered.

In this paper, we rely on the approach presented in [40] and [41], but we make important steps forward in order to accommodate the more general design of nonlinear fluid viscous dampers and their supporting braces in a practical and computationally efficient optimization-based seismic retrofitting approach. In particular, we will consider damper-brace elements made of two linear springs and a nonlinear dashpot in series. In this way it will be possible to account for the stiffness of the braces and of the dampers, and for the damping property of the viscous dampers. As we will see, a more rigorous formulation of the manufacturing cost of the dampers is considered, based on the dampers' peak forces. Additionally, the gradient-based optimization algorithm is improved by considering a modified objective function, and by adding a post processing phase which allows to achieve more discrete and practical final designs. The dampers and their supporting braces are distributed in given structures and sized, selecting their sizes from a limited set of available size-groups. Each size-group is characterized by damper-brace elements with the same mechanical properties. The size-groups are limited in number to achieve final practical designs, but their properties are not predefined and are optimized simultaneously within a single problem formulation. The objective function to be minimized is the realistic retrofitting cost function presented in [41], which has been further enhanced due to the new problem formulation considered in this paper. Inter-story drifts at the peripheries are constrained to allowable values. These are evaluated with nonlinear time-history analyses considering an ensemble of realistic ground motions. Initially, the problem is formulated as a mixed-integer optimization problem, and it is solved with genetic algorithms (GA). Subsequently, the initial mixed-integer problem formulation is translated into a continuous one. This allows the solution of the nonlinear programming problem through a gradient-based approach, which reduces significantly the computational cost required for its solution. Final practical designs are achieved by means of material interpolation functions. These are interpolation schemes extensively applied in the context of structural topology optimization, which lately proved to be effective also in the context of seismic retrofitting with fluid viscous dampers based on optimization [40, 41]. Since the problem at hand is highly nonlinear and nonconvex, and the optimization is performed with an evolutionary algorithm (i.e. the genetic algorithm) and with a gradient-based algorithm, there is no formal guarantee of optimality in a global sense of the solutions achieved with both approaches.

The remainder of the article is organized as follows: In Sect. 2 we present the governing equations of the problem; The mixed-integer programming problem formulation is introduced in Sect. 3, with details on the design variables, the performance index, and the cost function considered; In Sect. 4 the mixed-integer programming problem is reformulated into a continuous optimization problem. The details for this transformation are given in specific sections; Finally, in Sect. 5 several results regarding the optimization of realistic irregular frames are presented, including a comparison between the results achieved with a genetic and a gradient-based algorithm; In Sect. 6 some final considerations and conclusions are drawn.

2 Governing equations

In this section, we present the governing equations for the dynamic equilibrium of a structure coupled with an added damping system. We first present the model used for the characterization of the damper-brace behavior. Subsequently, we focus on the system of differential equations of motion for a structure equipped with nonlinear fluid viscous dampers and supporting braces.

2.1 Damper-brace system characterization

In this work we consider damper-brace systems made of two springs and a dashpot in series, as shown in Figure 1. The first spring accounts for the stiffness of the supporting brace, while the second for the stiffness of the damper. Last, the dashpot accounts for the damping property of each fluid viscous

damper. The two springs are modeled with a linear force-displacement behavior, while the dashpot force-velocity behavior is defined by a fractional power law:

$$f_b = k_b u_b; \quad f_d = k_d u_d; \quad f_d = c_d sgn(\dot{u}_d) |\dot{u}_d|^\alpha \tag{2}$$

where f_b is the force in the brace, and f_d is the force in the damper; k_b is the brace stiffness, k_d the damper stiffness, and c_d its damping coefficient; u_b is the elongation of the brace, u_d the elongation of the damper, and $\dot{u}_d$ the relative velocity between the ends of the damper. The exponent $0 < \alpha \leq 1$ characterizes the nonlinear behavior of the dashpot. For α equal to one the damper is linear, while for α that tends to zero the formulation mimics the behavior of a friction damper. The exponent α significantly affects the computational effort required for integrating the equations of motion. The algorithm for the time-history analysis developed by the authors and used in this work successfully solved the equations of motion for values of α between 0.1 and 1. Due to equilibrium, the forces in the damper and in the brace are equal ($f_b = f_d$). It follows that:

$$k_b u_b = k_d u_d = c_d sgn(\dot{u}_d) |\dot{u}_d|^\alpha \tag{3}$$

The axial stiffness of a brace can be easily calculated. The stiffness contribution of a fluid viscous damper, on the contrary, is far less intuitive. It depends in fact on:

- The stiffness of the metal parts of the damper from one end to the other;

- The stiffness of the fluid column inside the damper;

- The expansion of the damper cylinder under pressure (which makes the fluid seem more compressible).

Among the three components above mentioned, the second is the more complex to be defined. The fluid under pressure behaves according to its bulk modulus curve, which is nonlinear. However, dampers of a single manufacturer typically have their peak forces at similar limit pressures, and in general they are also made of the same materials [42]. Thanks to this, many of the variables drop out and the estimation of the dampers' stiffness becomes more simple. For example, the end to end stiffness of a fluid viscous damper, as tested by Taylor Devices [42], is such that it reaches its rated force with an elongation u_d (Eq. (2)) of approximately 3% of its rated stroke. This defines the stiffness of the damper that can be considered as a constant property of the device.

The ratio between the damping coefficient of a damper, and the stiffness of the damper and the brace is very important in the solution of the equations of motion. In fact, it characterizes how the deformation demand is distributed between the dampers and the supporting braces. On this aspect depends also the complexity of the integration technique required in each time step. For this reason, we define a ratio between the damping coefficient of the dashpot and the equivalent stiffness resulting from the brace and the damper. To pre-assign a reasonable value for this ratio, we consider the structure subject to a ground acceleration. We can thus calculate the maximum inter-story drift (d_{max}) experienced by the given structure. Then, we isolate a damper-brace element, and we subject it to an harmonic displacement history, with amplitude d_{max}, and a frequency $\bar{\omega}$ equal to the first natural frequency of the structure that is above $4\,Hz$. It is known, in fact, that dampers behave as pure dashpots for exciting frequencies below a cut-off frequency of approximately $4\,Hz$ [4]. At the maximum force (F_{max}) experienced under this harmonic loading, we assume that the damper will have a displacement between its ends equal to the 3% of its maximum stroke (Δ_s). For the same force, we assume also that the brace will reach an elongation u_b equal to its ultimate displacement allowed (u_y). That is, at the maximum force F_{max} in the damper-brace system we have that: The brace stiffness is $k_b = \frac{F_{max}}{u_y}$; The damper stiffness is $k_d = \frac{F_{max}}{3\% \Delta_s}$.

With regards to the brace, considering for example a brace with length $L_b = 7000\,mm$ and made of FE360 steel: $u_y = \epsilon_y L_b = \frac{f_y}{E_s} L_b = \frac{235 MPa}{210 GPa} 7000\,mm = 7.8\,mm$, where ϵ_y is the axial deformation of the brace corresponding to the ultimate elongation u_y, f_y is the yielding stress, and E_s is the Young's modulus. For the damper we consider a rated stroke of $\Delta_s = \pm 4\,inches = \pm 10.16\,cm$. Hence, the equivalent end-to-end stiffness of the damper-brace system which accounts for the deformability of both
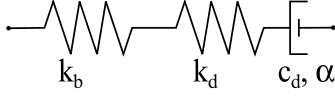
Figure 1: Stiffening and damping contributions of the initial damper-brace model.

Figure 2: Equivalent damper-brace model.

the brace and the damper can be calculated as follows:

$$k_{eq} = \frac{F_{max}}{u_b + u_d} = \frac{F_{max}}{\epsilon_y L_b + 3\% \, \Delta_s} = \frac{F_{max}}{7.8 \, mm + 3.05 \, mm} \cong \frac{c_d |\dot{u}_{max}^d|^\alpha}{10 \, mm} \tag{4}$$

where $\dot{u}_{max}^d$ is the maximum relative velocity measured between the dashpot ends under the harmonic loading considered. In particular, the ratio ρ is:

$$\rho = \frac{k_{eq}}{c_d} = 0.1 \, |\dot{u}_{max}^d|^\alpha = 0.1 \, \frac{F_{max}}{c_d} \tag{5}$$

It should be noted that ρ is measured in $\frac{1}{mm} \left(\frac{mm}{s} \right)^\alpha$. In Eq. (5), both ρ and $\dot{u}_{max}^d$ are unknown, because they depend one upon each other. Through the following iterative procedure it is possible to evaluate both of them:

1. Fix the values of c_d and α, and initialize ρ (e.g. $\rho = 1 \frac{1}{mm} \left(\frac{mm}{s} \right)^\alpha$);

2. Subject the damper-brace element to the harmonic displacement history $u(t) = d_{max} sin(\bar{\omega}t)$, and evaluate F_{max};

3. Update ρ through the Eq. (5).

The steps 2 and 3 are repeated until the update of ρ between two consecutive iterations $i - 1$ and i becomes sufficiently small (e.g. $\frac{\rho_i - \rho_{i-1}}{\rho_{i-1}} \leq 10^{-10}$). Once the ratio ρ is defined, we express k_{eq} as (Figure 2):

$$k_{eq} = \rho \, c_d \tag{6}$$

Therefore, for each damper-brace element the damping coefficient c_d is the design variable, for a given ratio ρ and exponent α.

2.2 Equations of motion

We consider generic 3-D irregular frames subject to an ensemble of realistic ground motions. Their behavior is characterized by the mass matrix $\mathbf{M}$, the inherent damping matrix $\mathbf{C}_s$, and the stiffness matrix $\mathbf{K}_s$. Nonlinear damper-brace elements are distributed in predefined potential locations of the structure. They all share the same ratio ρ, and exponent α, that have been already presented in Sec. 2.1. Each damper is characterized by a specific damping coefficient c_d.

The responses of interest are evaluated with nonlinear time-history analyses. For each point t in time, the dynamic behavior of a structure with N_{dof} degrees of freedom and N_d potential locations for dampers is defined by a set of N_{dof} second order differential equations, coupled with a set of N_d first order differential equations as follows:

$$\mathbf{M}\ddot{\mathbf{u}}(t) + \mathbf{C}_s\dot{\mathbf{u}}(t) + \mathbf{K}_s\mathbf{u}(t) + \mathbf{T}^T\mathbf{f}_d(t) = -\mathbf{M}\mathbf{e}a_g(t)$$

$$\dot{\mathbf{f}}_d(t) = \mathcal{D}(\mathbf{k}_{eq}) \left[\mathbf{T}\dot{\mathbf{u}}(t) - \left(\mathcal{D}(\mathbf{c}_d)^{-1}\mathcal{D}(|\mathbf{f}_d(t)|) \right)^{\frac{1}{\alpha}} sgn(\mathbf{f}_d(t)) \right] \tag{7}$$

In Eq. (7) $\mathbf{u}(t)$, $\dot{\mathbf{u}}(t)$, and $\ddot{\mathbf{u}}(t)$ are the displacement, velocity, and acceleration vectors of the degrees of freedom relatively to the ground at time t; $\mathbf{f}_d(t)$ is the vector of the resisting forces of the dampers at time t; $\mathbf{e}$ is the vector that defines the location of the excitation; and $a_g(t)$ is the ground acceleration as a function of time. $\mathcal{D}(\cdot)$ is an operator that transforms a vector into a diagonal matrix, and a diagonal matrix into a vector (as the `diag(·)` MATLAB function does). The matrix $\mathbf{T}$ is a transformation matrix,

5

that transforms the global coordinates for the displacements and velocities $(\mathbf{u}, \dot{\mathbf{u}})$ into local damper-brace coordinates $(\mathbf{d}^L, \dot{\mathbf{d}}^L)$. The readers are referred to [57] for a similar transformation of coordinates.

In order to be solved, the problem is first discretized in time, and then solved with the Newmark-β method. In particular, in each time step the equilibrium is achieved by means of an iterative procedure. In this procedure, in each step the dampers' forces are approximated with a fourth-order explicit Runge-Kutta method, as suggested in [43, 44]. For more details on Runge-Kutta methods the readers are referred to [45]. The structural response is then corrected with the Newton-Raphson method. The iterative procedure stops when the residual forces in each time-step are smaller or equal to a predefined tolerance (e.g. 10^{-6}).

3   Optimization problem formulation

In the following section, we first present the design variables involved in the problem formulation, which play an important role in achieving final discrete and practical designs. Then, the retrofitting cost function minimized in the optimization is introduced. Last, the constrained performance indices are presented.

3.1   Design variables

The goal is to size and distribute nonlinear fluid viscous dampers and their supporting braces in N_d predefined potential locations of a given frame. The damper-brace elements can be chosen out of two available size-groups, where for size-group we intend a group of elements with the same characteristics. Thus, as we explained in Sec. 2.1, we have to determine the damping coefficients $c_{d,i}$, that are collected in the vector $\mathbf{c}_d$. The vector of damping coefficients is defined as follows:

$$\mathbf{c}_d = \bar{c}_d \mathcal{D}(\mathbf{x}_1)(y_1 \mathbf{1} + (y_2 - y_1)\mathbf{x}_2) \tag{8}$$

In Eq. (8), $\bar{c}_d$ represents the maximum damping coefficient available, and it is defined a priori. The vector $\mathbf{1}$ has unit entries and size $N_d \times 1$. The vector $\mathbf{x}_1$ has binary entries representing the existence of a damper in each potential locations. In particular, a value of zero in the i-th entry of the vector means that in the location i there is no damper, while a value of one that there is a damper. Also $\mathbf{x}_2$ is a vector with binary entries, and it represents the association of each existing damper to one of the two available size-groups. In the case of $x_{2,i}$ equal to zero, the damper in the i-th location belongs to the first size-group. In the case of $x_{2,i}$ equal to one, the damper in the i-th location belongs to the second size-group. The dimensions of the vectors $\mathbf{c}_d$, $\mathbf{x}_1$, and $\mathbf{x}_2$ are $N_d \times 1$.

The two available damping coefficients that characterize the two size-groups are:

$$\bar{c}_1 = \bar{c}_d y_1; \quad \bar{c}_2 = \bar{c}_d y_2 \tag{9}$$

In Eq. (9), y_1 and y_2 are two continuous design variables that scale the maximum available damping coefficient $\bar{c}_d$. The column vector $\mathbf{x}$ collects all the variables of the problem: $\mathbf{x}^T = \begin{bmatrix} \mathbf{x}_1^T, \mathbf{x}_2^T, y_1, y_2 \end{bmatrix}$. Last, it should be noted that the design indirectly extends also to the dampers' supporting braces through the parameter ρ, as has been illustrated in Sec. 2.1.

3.2   Cost function

In the work presented in this paper, we minimize a comprehensive formulation of the initial retrofitting cost. This formulation resembles the one presented in [41], even though, as we will see, it has been modified in order to formulate more rigorously the dampers' cost. In recent work [46, 47, 48], the life-cycle cost has been taken as the objective function to be minimized in similar design problems. These cost formulations accounted for the initial, maintenance, and failure costs. In our approach, instead, we focus only on the initial cost, considering a more complete formulation of this cost component.

Thus, also in this case the cost function J consists of three cost components:

$$J = J_l + J_m + J_p \tag{10}$$

The first and third cost components (i.e. J_l and J_p) have been proposed in [41]. The second cost component (i.e. J_m) resembles the one presented in [41], but it is further enhanced in order to formulate the manufacturing cost of the dampers based on their peak forces rather than on their damping coefficients.

In particular, the first cost component J_l represents the cost associated with the number of locations in which dampers are installed. We allow the algorithm to allocate as many as one damper in each potential location; hence, this component includes all costs associated with the preparation of the structure for the damper installation and the architectural constraint that this installation will represent. Moreover, in case of retrofitting, it can also account for the removal of existing nonstructural components. The first component of the cost is defined as follows:

$$J_l = \mathbf{C}_l^T \mathbf{x}_1 \tag{11}$$

where $\mathbf{C}_l$ is a $N_d \times 1$ vector in which the i-th component is a cost component related to the i-th component of $\mathbf{x}_1$.

The second cost component, J_m, represents the manufacturing cost of the dampers. In principle, the manufacturing cost of viscous dampers depends on the peak stroke and on the square root of the peak force of the most loaded damper of each size-group [42]. We assume, in fact, that all dampers of a specific size-group are designed so to have the same capacity. Since we are constraining inter-story drifts, also the peak stroke of the dampers is indirectly limited. As a consequence, it does not affect significantly the cost. Therefore, the manufacturing cost is defined as the square root of the peak force of the most loaded damper from each size-group, multiplied by the number of dampers of the corresponding size-group. Formally, it is written as follows:

$$J_m = C_m \left\{ \mathbf{x}_1^T (\mathbf{1} - \mathbf{x}_2) \left[\max_i \left(\hat{f}_{d1,i} \right) \right]^{0.5} + \mathbf{x}_1^T \mathbf{x}_2 \left[\max_i \left(\hat{f}_{d2,i} \right) \right]^{0.5} \right\} \tag{12}$$

where C_m is a coefficient used to homogenize the units of measure of J_m to the units of measure of J_l and J_p, $\mathbf{x}_1^T (\mathbf{1} - \mathbf{x}_2)$ is the number of dampers of the first size-group, $\mathbf{x}_1^T \mathbf{x}_2$ is the number of dampers of the second size-group, and:

$$\begin{aligned}
\hat{\mathbf{f}}_{d1} &= \begin{bmatrix} \hat{f}_{d1,1} & \cdots & \hat{f}_{d1,i} & \cdots & \hat{f}_{d1,N_d} \end{bmatrix}^T = \mathcal{D} (\mathbf{1} - \mathbf{x}_2) \hat{\mathbf{f}}_d \\
\hat{\mathbf{f}}_{d2} &= \begin{bmatrix} \hat{f}_{d2,1} & \cdots & \hat{f}_{d2,i} & \cdots & \hat{f}_{d2,N_d} \end{bmatrix}^T = \mathcal{D} (\mathbf{x}_2) \hat{\mathbf{f}}_d; \quad \hat{\mathbf{f}}_d = \max_t (|\mathbf{f}_d(t)|)
\end{aligned} \tag{13}$$

$\hat{\mathbf{f}}_d$ is the vector of the peak forces in time for all dampers; the vector $\hat{\mathbf{f}}_{d1}$ has the components of $\hat{\mathbf{f}}_d$ which belongs to dampers of the first size-group, while $\hat{\mathbf{f}}_{d2}$ those of the second size-group.

Modern seismic codes require to test one damper prototype from each size-group so to verify its force-velocity behavior. As a results, we consider an additional cost component, J_p. This component is formulated so that the number of different size-groups of dampers used for retrofitting should be minimized:

$$J_p = C_p \left[\mathcal{H}(\mathbf{x}_1^T (\mathbf{1} - \mathbf{x}_2)) + \mathcal{H}(\mathbf{x}_1^T \mathbf{x}_2) \right]; \quad \mathcal{H}(x) = \begin{cases} 1 \text{ for } x > 0 \\ 0 \text{ for } x = 0 \end{cases} \tag{14}$$

where C_p is the cost of prototype testing and design. The function $\mathcal{H}$ is the Heaviside step function. We observe that: If all dampers are of the first size then J_p will be equal to $C_p \times [1 + 0]$; If all dampers are of the second size then J_p will be equal to $C_p \times [0 + 1]$; In case dampers of both sizes exist then J_p will be equal to $C_p \times [1 + 1]$.

3.3 Performance index

We are now considering the seismic retrofitting of 3-D irregular frames using nonlinear fluid viscous dampers. As in [40], here too inter-story drifts are used as an appropriate measure of both structural and nonstructural damage levels. Moreover, limiting the inter-story drifts enforces the assumption of linear elastic behavior of the structure. This can be done by limiting the inter-story drifts to the value of drift for which yielding occurs.

In particular, the peak inter-story drift normalized by the allowable value is chosen as the local performance index for 2-D irregular frames:

$$d_{c,i} = \max_t(|d_i(t)/d_{allow}|) \leq 1 \quad \forall i = 1, \ldots, N_{drifts} \tag{15}$$

where the inter-story drift $d_i(t)$ is the i-th constrained inter-story drift at time t; d_{allow} its maximum allowable value. In the case of 3-D frames, $d_i(t)$ refers to the inter-story drifts of peripheral frames.

3.4 Mixed-integer optimization problem

At this point we have presented all the ingredients of our optimization problem. The following is its mixed-integer formulation:

$$
\begin{aligned}
\min_{\mathbf{x}} \quad & J = J_l + J_m + J_p \\
\text{s. t.:} \quad & d_{c,i} = \max_t(|d_i(t)/d_{allow}|) \leq 1 \quad \forall i = 1, \ldots, N_{drifts} \\
& x_{1,k} = \{0,1\} \quad k = 1, \ldots, N_d \\
& x_{2,k} = \{0,1\} \quad k = 1, \ldots, N_d \\
& 0 \leq y_1 < y_2 \leq 1 \\
\text{with} \quad & \mathbf{M}\ddot{\mathbf{u}}(t) + \mathbf{C}_s\dot{\mathbf{u}}(t) + \mathbf{K}_s\mathbf{u}(t) + \mathbf{T}^T\mathbf{f}_d(t) = -\mathbf{M}\mathbf{e}a_g(t), \; \forall \mathbf{a}_g(t) \in \mathcal{E} \\
& \dot{\mathbf{f}}_d(t) = \mathcal{D}(\mathbf{k}_{eq}) \left[\mathbf{T}\dot{\mathbf{u}}(t) - \left(\mathcal{D}(\mathbf{c}_d)^{-1} \mathcal{D}(|\mathbf{f}_d(t)|) \right)^{\frac{1}{\alpha}} sgn(\mathbf{f}_d(t)) \right] \\
& \mathbf{u}(0) = 0, \quad \dot{\mathbf{u}}(0) = 0, \quad \mathbf{f}_d(0) = 0 \\
& \mathbf{c}_d = \bar{c}_d \mathcal{D}(\mathbf{x}_1)(y_1\mathbf{1} + (y_2 - y_1)\mathbf{x}_2), \; \mathbf{k}_{eq} = \rho\mathbf{c}_d
\end{aligned} \tag{16}
$$

where $\mathcal{E}$ is an ensemble of ground motions considered; and N_{drifts} is the number of drifts to be constrained. For optimizing the distribution and size of a single damper size-group, only the $\mathbf{x}_1$ and y_1 variables are necessary, thus it can be seen as a particular case. The problem (16) has been solved with a GA. The results will be used for comparison in Sec. 5.

4 Gradient-based optimization

In order to reduce the computational effort required for the solution of the problem, we reformulate the mixed-integer problem (16) with a continuous approximation of the problem. To this end, first we introduce the material interpolation functions used to promote the convergence towards final discrete solutions. The continuous problem is solved with an algorithm based on first-order information. Hence, all the functions involved need to be continuously differentiable. For this reason, we approximate two cost components, and the constraints with differentiable formulations. In particular we aggregate the constraints into one single constraint. This reduces the number of additional analyses required for the evaluation of the gradients, and as a consequence the computational cost of the sensitivity analysis.

4.1 Damping penalization

We are now reformulating the problem with continuous variables only. One of the main consequences is that all the variables can now assume all the values between their upper and lower bounds. Looking at the vectors of variables $\mathbf{x}_1$ and $\mathbf{x}_2$, we understand that their intermediate values should be avoided. Hence, we introduce in the problem formulation the so-called material interpolation functions. These functions have been successfully apllied in the field of structural topology and discrete material optimization. Among them, SIMP (Solid Isotropic Material with Penalization) is the most popular and has proved to be very effective in a wide range of applications [49, 50]. Its main idea is to penalize the intermediate values of binary variables making them uneconomical, thus implicitly leading the optimizer towards a preference of 0-1 values (in our problem, looking for instance at the i-th entry of the vector $\mathbf{x}_1$, this would mean that a damper either does not exist or it does exist, respectively). Similarly, also RAMP (Rational

Approximation of Material Properties) is a material interpolation function based on the same main idea [51].

Very recently, the material interpolation functions have been introduced also in the context of optimization-based seismic retrofitting. In particular, RAMP proved to be very effective for achieving final discrete solutions [40, 41]. In the optimization problem presented herein, both SIMP and RAMP were tested in the formulation of the damping coefficients (8). However, SIMP was chosen for the final problem formulation since it proved to be more effective and promising in leading the optimizer towards final discrete solutions. In this case, in fact, a combination of two SIMP functions has been applied to the vectors $\mathbf{x}_1$ and $\mathbf{x}_2$ in the damping formulation as follows [52, 53, 54, 55]:

$$\tilde{c}_{d,i} = c_{d0} + \bar{c}_d \, x_{1,i}^p \left(y_1 + (y_2 - y_1) \, x_{2,i}^p \right), \quad i = 1, \ldots, N_d \tag{17}$$

where c_{d0} represents an artificial value of damping, and it avoids numerical issues with the Runge-Kutta approximation used during the integration of the equations of motion. In the work discussed in this paper c_{d0} is set to 10^{-6}. In Eq. (17) for $p = 1$ we have a linear interpolation of the damping. For increasing values of p, the penalizing effect on the values of $\mathbf{x}_1$ and $\mathbf{x}_2$ between zero and one increases. This indirectly leads to final 0-1 optimal solutions.

4.2 Cost function reformulation

An important step for the reformulation of (16) into a continuous problem is the approximation of the cost components J_m and J_p with differentiable formulations.

In the second cost component J_m we need first to approximate $\max_t \left(|\mathbf{f}_d(t)| \right)$ (Eq. (13)) with a r-norm formulation:

$$\tilde{\mathbf{f}}_d = \left(\frac{1}{t_f - t_0} \int_{t_0}^{t_f} \mathcal{D} \left(\mathbf{f}(t) \right)^r dt \right)^{\frac{1}{r}} \mathbf{1} \tag{18}$$

where r is a large even number. Then, we substitute $\max_i \left(\hat{f}_{d1,i} \right)$, and $\max_i \left(\hat{f}_{d2,i} \right)$ (Eq. (12)) with two differentiable weighted averages:

$$\tilde{J}_m = C_m \left\{ \mathbf{x}_1^T (\mathbf{1} - \mathbf{x}_2) \left[\frac{\mathbf{1}^T \mathcal{D} \left(\tilde{\mathbf{f}}_{d1} \right)^{q+1} \mathbf{1}}{\mathbf{1}^T \mathcal{D} \left(\tilde{\mathbf{f}}_{d1} \right)^q \mathbf{1}} \right]^{0.5} + \mathbf{x}_1^T \mathbf{x}_2 \left[\frac{\mathbf{1}^T \mathcal{D} \left(\tilde{\mathbf{f}}_{d2} \right)^{q+1} \mathbf{1}}{\mathbf{1}^T \mathcal{D} \left(\tilde{\mathbf{f}}_{d2} \right)^q \mathbf{1}} \right]^{0.5} \right\} \tag{19}$$

where:

$$\tilde{\mathbf{f}}_{d1} = \mathcal{D} \left(\mathbf{1} - \mathbf{x}_2 \right) \tilde{\mathbf{f}}_d; \quad \tilde{\mathbf{f}}_{d2} = \mathcal{D} \left(\mathbf{x}_2 \right) \tilde{\mathbf{f}}_d \tag{20}$$

When q is large the weighted average functions approach the maximal components of $\tilde{\mathbf{f}}_{d1}$ and $\tilde{\mathbf{f}}_{d2}$. Unfortunately, the formulation (19) did not work as we expected. The optimizer seemed to consider as variables only $\mathbf{x}_1$ and $\mathbf{x}_2$, without modifying y_1 and y_2. The reason for this undesired behavior could be that the variations $\Delta\mathbf{x}_1$ and $\Delta\mathbf{x}_2$ affected more the value of the objective function rather than Δy_1 and Δy_2. This problem was not encountered in [41], where the manufacturing cost considered for linear fluid viscous dampers was based on their damping coefficient. In that case, in fact, the results showed a good convergence to final discrete designs. Therefore, to avoid any prioritization between the design variables, and motivated by the results presented in [41], we reformulated the cost component $\tilde{J}_m$ as follows:

$$\tilde{J}_m = C_m \mathbf{1}^T \left\{ \mathbf{1} f_{d0} + \bar{c}_d \mathcal{D} \left(\mathbf{x}_1 \right) \left(\mathbf{1} y_1 + (y_2 - y_2) \mathbf{x}_2 \right) V_{max}^{g1} + \right. $$
$$\left. + \mathcal{D} \left(\mathbf{x}_2 \right) \bar{c}_d \mathcal{D} \left(\mathbf{x}_1 \right) \left(\mathbf{1} y_1 + (y_2 - y_2) \mathbf{x}_2 \right) \left(V_{max}^{g2} - V_{max}^{g1} \right) \right\}^{0.5} \tag{21}$$

where f_{d0} is an artificial value of damper force set to 10^{-6}, and it was needed to avoid numerical issues in the objective function gradient. In (21), V_{max}^{g1} and V_{max}^{g2} are the ratios between the maximum peak force and the damping coefficient of each size-group. They have constant values for a given value of

penalization p in Eq. (17), and when p is increased V_{max}^{g1} and V_{max}^{g2} are updated. The details regarding how the penalization p varies in the optimization process will be discussed in a later section. However, since V_{max}^{g1} and V_{max}^{g2} have constant values they do not affect the gradient of the objective function. More precisely, these two parameters are defined as follows:

$$V_{max}^{g1} = \max \left[\mathcal{D} \left(\mathbf{1} - \mathbf{x}_2 \right) \mathcal{D}^{-1} \left(\tilde{\mathbf{c}}_d \right) \tilde{\mathbf{f}}_d \right]; \quad V_{max}^{g2} = \max \left[\mathcal{D} \left(\mathbf{x}_2 \right) \mathcal{D}^{-1} \left(\tilde{\mathbf{c}}_d \right) \tilde{\mathbf{f}}_d \right] \tag{22}$$

where the max function in (22) evaluates the maximal component of the vectors between square brackets. V_{max}^{g1} and V_{max}^{g2} can also be seen as surrogate maximum velocities between the ends of the dampers of the first and second size-group, respectively. With reference to the nonlinear force-velocity behavior of the dampers (Eq. (2)), they resemble the following definition:

$$V = \frac{f_d}{c_d} = sgn(\dot{u}_d) \, |\dot{u}_d|^\alpha \tag{23}$$

In this way, Eq. (21) represents the square root of the peak force of the most loaded damper from each size group, multiplied by the number of dampers of the corresponding size-group. Additionally, $\tilde{J}_m$ formulated as in Eq. (21) is convenient also from a computational point of view. In fact, it is formulated explicitly in terms of the variables of the problem, and its gradient can be calculated directly without requiring an additional adjoint sensitivity analysis.

In the third cost component J_p, the Heaviside step function needs to be regularized in order to be continuously differentiable. As in [41], this is done through the exponential function presented in [56]:

$$\tilde{\mathcal{H}}(x) = 1 - \exp(-\beta \, x) + x \exp(-\beta). \tag{24}$$

For $\beta = 0$ the function $\tilde{\mathcal{H}}$ is linear, and it tends to match the Heaviside step function as β increases. Considering Eq. (24), J_p becomes:

$$\begin{aligned} \tilde{J}_p &= C_p \left[\tilde{\mathcal{H}}(\mathbf{x}_1^T (\mathbf{1} - \mathbf{x}_2)/N_d) + \tilde{\mathcal{H}}(\mathbf{x}_1^T \mathbf{x}_2/N_d) \right] = \\ &= C_p [(1 - \exp(-\beta \mathbf{x}_1^T (\mathbf{1} - \mathbf{x}_2)/N_d) + (\mathbf{x}_1^T (\mathbf{1} - \mathbf{x}_2)/N_d)\exp(-\beta)) + \\ &+ (1 - \exp(-\beta \mathbf{x}_1^T \mathbf{x}_2/N_d) + (\mathbf{x}_1^T \mathbf{x}_2/N_d)\exp(-\beta))] \end{aligned} \tag{25}$$

4.3 Aggregated constraint

As we saw previously with regards to the second cost component, also the $\max_t$ function in (15) is non differentiable. Therefore, we reformulate also $\mathbf{d}_c$ from Eq. (15) with a r-norm differentiable formulation [57]:

$$\tilde{\mathbf{d}}_c = \left(\frac{1}{t_f - t_0} \int_{t_0}^{t_f} (\mathcal{D}^{-1}(\mathbf{d}_{allow}) \mathcal{D}(\mathbf{Hu}(t)))^r dt \right)^{\frac{1}{r}} \mathbf{1} \tag{26}$$

where $\mathbf{H}$ is a matrix that transforms the global displacements ($\mathbf{u}$) into the constrained inter-story drifts. It should be noted that for a given moment in time $\bar{t}$, the result of the prouct $\mathcal{D}^{-1}(\mathbf{d}_{allow}) \mathcal{D}(\mathbf{Hu}(\bar{t}))$ is also a diagonal matrix. Also in Eq. (26) r is a large even number. Subsequently we reduce the number of constraints to one, so to reduce the computational effort required in the sensitivity analysis from N_{drifts} analyses to one. In particular, we introduce the following aggregated inter-story drift constraint:

$$\tilde{d}_c = \frac{\mathbf{1}^T D^{q+1} \left(\tilde{\mathbf{d}}_c \right) \mathbf{1}}{\mathbf{1}^T D^q \left(\tilde{\mathbf{d}}_c \right) \mathbf{1}} \tag{27}$$

As we already mentioned, when q is a large number the weighted average (27) approaches the maximal component of the vector $\tilde{\mathbf{d}}_c$.

4.4 Final continuous optimization problem and sensitivity analysis

Finally, the continuous approximation of the optimization problem is the following:

$$\min_{\mathbf{x}} \quad \tilde{J} = J_l + \tilde{J}_m + \tilde{J}_p$$

$$\text{s. t.:} \quad \tilde{d}_c = \frac{\mathbf{1}^T D^{q+1}\left(\tilde{\mathbf{d}}_c(t_f)\right)\mathbf{1}}{\mathbf{1}^T D^q\left(\tilde{\mathbf{d}}_c(t_f)\right)\mathbf{1}} \leq 1$$

$$0 \leq x_{1,k} \leq 1 \quad k = 1,\dots,N_d$$

$$0 \leq x_{2,k} \leq 1 \quad k = 1,\dots,N_d$$

$$0 \leq y_1 < y_2 \leq 1$$

$$\text{with} \quad \mathbf{M}\ddot{\mathbf{u}}(t) + \mathbf{C}_s\dot{\mathbf{u}}(t) + \mathbf{K}_s\mathbf{u}(t) + \mathbf{T}^T\mathbf{f}_d(t) = -\mathbf{M}\mathbf{e}a_g(t), \ \forall \mathbf{a}_g(t) \in \mathcal{E}$$

$$\dot{\mathbf{f}}_d(t) = \mathcal{D}\big(\tilde{\mathbf{k}}_{eq}\big)\left[\mathbf{T}\dot{\mathbf{u}}(t) - \left(\mathcal{D}\big(\tilde{\mathbf{c}}_d\big)^{-1}\mathcal{D}\big(|\mathbf{f}_d(t)|\big)\right)^{\frac{1}{\alpha}} sgn(\mathbf{f}_d(t))\right]$$

$$\mathbf{u}(0) = 0, \quad \dot{\mathbf{u}}(0) = 0, \quad \mathbf{f}_d(0) = 0$$

$$\tilde{\mathbf{c}}_d = c_{d0}\mathbf{1} + \bar{c}_d\,\mathcal{D}(\mathbf{x}_1^p)\,(y_1\mathbf{1} + (y_2 - y_1)\,\mathbf{x}_2^p)\,, \ \tilde{\mathbf{k}}_{eq} = \rho\tilde{\mathbf{c}}_d$$

$$\tilde{\mathbf{d}}_c = \left(\frac{1}{t_f}\int_0^{t_f}(\mathcal{D}^{-1}(\mathbf{d}_{allow})\mathcal{D}(\mathbf{H}\mathbf{u}(t)))^r dt\right)^{\frac{1}{r}}\mathbf{1}$$

(28)

where for $\mathbf{x}_1 \in \mathbb{R}^{N_d}$, $\mathbf{x}_1^p = \left[x_{1,1}^p \ \dots \ x_{1,N_d}^p\right]^T$. The same definition applies to $\mathbf{x}_2^p$.

The problem (28) has been solved with a modified sequential linear programming approach (SLP), inspired by the cutting planes method [58, 59]. More details regarding the algorithm will be given in a later section. With this method, in every optimization cycle a linearized sub-problem is solved. Therefore, first-order derivatives of the objective function and of the aggregated inter-story drift constraint are needed. The calculation of the objective function gradient in (28) (i.e. $\frac{\partial \tilde{J}}{\partial \mathbf{x}}$) is straight forward, because it is formulated directly in terms of the variables of the problem. The gradient of the aggregated constraint (i.e. $\frac{\partial \tilde{d}_c}{\partial \mathbf{x}}$), on the other hand, requires an adjoint sensitivity analysis. To ensure the consistency of the sensitivity calculated, we relied on the discretize-then-differentiate adjoint variable method [60, 61, 62]. Essentially, in this procedure we expand the discretized general constraint by adding to it zero terms multiplied by adjoint variables. The zero terms are all the equations that must be satisfied to guarantee the equilibrium in each time step. Then, the resulting discrete function is differentiated. The unknown response derivatives are eliminated by collecting and equating to zero the terms multiplied by them. This results in a set of transient linear equations where the unknowns are the adjoint variables. Once these equations are solved it is possible to calculate the sensitivity through the adjoint variables. A more detailed description of this cumbersome procedure would be out of the scope of this paper. Ultimately, the adjoint sensitivity analysis procedure results in the evaluation of the vector $\frac{\partial \tilde{d}_c^T}{\partial \mathbf{c}_d} = \left[\frac{\partial \tilde{d}_c}{\partial c_{d\,1}} \ \dots \ \frac{\partial \tilde{d}_c}{\partial c_{d\,N_d}}\right]$, and the complete derivatives are computed with the chain rule:

$$\frac{\partial \tilde{d}_c}{\partial \mathbf{x}_1} = \frac{\partial \mathbf{c}_d}{\partial \mathbf{x}_1}\frac{\partial \tilde{d}_c}{\partial \mathbf{c}_d}; \quad \frac{\partial \tilde{d}_c}{\partial \mathbf{x}_2} = \frac{\partial \mathbf{c}_d}{\partial \mathbf{x}_2}\frac{\partial \tilde{d}_c}{\partial \mathbf{c}_d}; \quad \frac{\partial \tilde{d}_c}{\partial y_1} = \frac{\partial \mathbf{c}_d}{\partial y_1}\frac{\partial \tilde{d}_c}{\partial \mathbf{c}_d}; \quad \frac{\partial \tilde{d}_c}{\partial y_2} = \frac{\partial \mathbf{c}_d}{\partial y_2}\frac{\partial \tilde{d}_c}{\partial \mathbf{c}_d}$$

(29)

4.5 Optimization algorithm

The optimization problem (28) is highly nonlinear and nonconvex. Therefore, in what follows we discuss several precautions that we included in the optimization algorithm.

4.5.1 Continuation scheme

The optimization problem (28) is based on few nonlinear components that increase its complexity, such as: the penalized damping coefficients (17); the differentiable approximations of the max functions (26) and (27); the differentiable approximation of the Heaviside step function (24) used in the reformulation

11

of the third cost component (25). These components are characterized by the parameters p, s, r, q, β, that need to assume high values in order to produce meaningful approximations. Experience showed that it is convenient to increase these parameters gradually in a stepwise manner, known also as continuation scheme. In particular, the parameters p and s are increased by a fraction of their value every time a local convergence criterion in a continuation step is satisfied for a certain number of iterations. The criterion requires the norm of the variables' updates to be smaller than a certain tolerance for five consecutive iterations, that is: $\|\mathbf{x}_k - \mathbf{x}_{k-1}\| \leq \epsilon_{p,s}$. Moreover, a parametric study showed that it is more efficient to start the optimization analysis with limited but noticeable initial values of these parameters. The parameters r and q increase every iteration with a constant step-size; β is scaled by the coefficient s, which varies between zero and one. The coefficient s scales also the cost components $\mathbf{C}_l$ and C_p, so to progressively and smoothly include the first and third cost components in the objective function as the algorithm converges to a more and more discrete solution. Moreover, conservative moving limits are imposed in the solution of the linear subproblems. As a consequence, the updates of the variables $\mathbf{x}_1$, $\mathbf{x}_2$, y_1, y_2, are found in a neighborhood of the solution of the previous subproblem. Details regarding the specific values of these parameters are given in the numerical examples.

4.5.2 Management of the constraints

As we already mentioned, we solved (28) with a modified sequential linear programming approach inspired by the cutting planes method. In every iteration of standard sequential linear programming, a linear subproblem is solved. In the algorithm discussed herein, the subproblems expand, as in each iteration the new linearized constraint is added to the set of constraints considered. Due to the non-convexity of our problem, and in particular of the aggregated constraint, it may happen that a constraint is active even though the current solution strictly falls into the feasible domain. In other words, it may happen that a constraint cuts the feasible domain directing the algorithm towards too conservative solutions. This is clearly shown in Figure 2 of [36]. The sequential linear programming algorithm was modified in order to nullify and disregard these undesired constraints in the following iterations.

4.5.3 Convergence to a discrete solution

The problem that we solved was a penalized continuous optimization problem. Thus, for low initial values of the penalization the algorithm converged towards a continuous solution. Through the iterations, as the penalization (i.e. the parameter p) grew, the algorithm shifted its preference towards values, for the variables $\mathbf{x}_1$ and $\mathbf{x}_2$, more and more close to their boundaries. From initial results, we observed that the algorithm tended to be reluctant to converge to clean final discrete solutions, characterized by crisp distributions of 0-1 values for the vectors $\mathbf{x}_1$ and $\mathbf{x}_2$. To improve the convergence of our algorithm towards final binary solutions in terms of $\mathbf{x}_1$ and $\mathbf{x}_2$, we modified the objective function to be minimized:

$$J_{tot} = (1 - \frac{p}{p_{max}})\tilde{J} + \bar{c}_d \frac{p}{p_{max}} J_{binary} \tag{30}$$

where $\tilde{J}$ was presented in Sec. 4.2, and J_{binary} is defined as follows [63, 64]:

$$J_{binary} = \mathbf{x}_1^T(\mathbf{1} - \mathbf{x}_1) + \mathbf{x}_2^T(\mathbf{1} - \mathbf{x}_2) \tag{31}$$

The component J_{binary} is zero when all the values of $\mathbf{x}_1$ and $\mathbf{x}_2$ are binary. For intermediate values of $\mathbf{x}_1$ and $\mathbf{x}_2$, J_{binary} is different from zero and positive. J_{binary} is also multiplied by $\bar{c}_d$ so that numerically the two components of J_{tot} have comparable values. Essentially, the purpose of J_{binary} is to assist the material interpolation functions (Eq. (17)) in promoting final discrete solutions. In fact, for small values of the penalization p, the function to be minimized is $J_{tot} \cong \tilde{J}$. As a consequence, the algorithm is driven towards initial minimum-cost continuous design solutions. When the penalization grows, the intermediate values of $\mathbf{x}_1$ and $\mathbf{x}_2$ becomes inconvenient. Simultaneously, the influence of the component J_{binary} on the total cost increases, while the effect of $\tilde{J}$ decreases. For high values of p $J_{tot} \cong J_{binary}$, and the algorithm is pushed towards a preference of final solutions that are binary with respect to $\mathbf{x}_1$ and $\mathbf{x}_2$. This allows the translation of the initial continuous damping distribution into the closest mixed-integer equivalent.

As p grows and J_{binary} becomes more influential ($J_{tot} \cong J_{binary}$) it may happen that the algorithm increases the damping coefficients of the two size-groups since it can satisfy anyway the constraint with no additional cost. To avoid this, we progressively modify the upper and lower moving limits of the variables y_1 and y_2, in a way that for high values of p the bounds of y_1 and y_2 almost coincide with the current optimized values of y_1 and y_2.

4.5.4 Convergence criteria

The methodology is assumed to have reached the final optimized solution if: The parameter s equals $s_{max} = 1$; The norm of the update of the design variables in the current k-th iteration is smaller than a predefined value $||\mathbf{x}_k - \mathbf{x}_{k-1}||_2 \leq \epsilon$; The maximum normalized inter-story drift d_c is smaller or equal than the allowable one, d_{allow}, with a certain tolerance. More details regarding these parameters will be given in Sec. 5.

4.5.5 Post processing

At the end of the optimization analysis, the entries of $\mathbf{x}_1$ and $\mathbf{x}_2$ that are not exactly binary are rounded. As a consequence, it may happen that the optimality of the rounded solution is somehow spoiled, and that it violates the drift constraints or that it is too conservative. Therefore, we introduced a post processing phase where a new optimization is carried out. In this case the only variables are y_1 and y_2 for the given (rounded) $\mathbf{x}_1$ and $\mathbf{x}_2$. The objective function minimized is only the cost associated to the manufacturing of the dampers, $\tilde{J} = \tilde{J}_m$, because the other cost components are constant. For the remaining part, the optimization problem solved in the post processing phase is identical to (28).

5   Numerical examples

In the following section, several numerical results are presented and discussed. They have been obtained by optimizing two realistic structures. As already mentioned, the continuous formulation (28) was solved with a modified SLP approach inspired by the cutting planes method, that was implemented in MATLAB by the authors. The mixed-integer formulation (16) was solved using MATLAB's built-in GA. The two formulations are compared in terms of results achieved and computational effort required.

In particular, we consider two examples of asymmetric frames made of reinforced concrete. The first was introduced in [65]. It was also solved in [57], where an optimal continuous damping was found, and in [40] and [41] but yielding a discrete damping distribution. For this example the coefficient ρ of the damper-brace elements (Sec. 2.1) was set to 1.0765. The second is a new example proposed by the authors of this paper. It is based on a modification of the geometry of the first. The result is a double setback irregular frame. In this case, the coefficient ρ of the damper-brace elements was set to 1.0867.

In both examples the column sizes are 0.5 m × 0.5 m in frames 1 and 2; 0.7 m × 0.7 m in frames 3 and 4 (see Figure 3 and Figure 4). The beam sizes are 0.4 m × 0.6 m and the floor mass is uniformly distributed with a weight of 0.75 $\left[\frac{ton}{m^2}\right]$. Regarding the ground motion acceleration, out of the ensemble LA 10% in 50 years [66], $LA16$ was considered first in both examples, acting in the y direction [57]. However, as we will see the proposed formulation can consider multiple acceleration records at once. In these examples, we consider 5% of critical damping for the first two modes in order to build the Rayleigh damping matrix of the structures. In Table 1 are presented the numerical values of several parameters involved in the problem formulation. It should be noted that the cost components of the vector $\mathbf{C}_l$ were all equal in the numerical experiments. Thus, in what follows $\mathbf{C}_l = C_l\mathbf{1}$, where $\mathbf{1}$ is a vector with N_d unit entries. Moreover, the coefficient β was used only in the SLP algorithm. In the GA, in fact, a true non-differentiable Heaviside step function was considered. Table 2 lists the initial and final values, and the step sizes through which the parameters of the continuation scheme of the SLP algorithm are initialized and increased.

In the SLP algorithm we defined three criteria for convergence to be satisfied simultaneously: The first requires the parameter s to reach its maximum value; The second requires the update of the variables $\mathbf{x}_k - \mathbf{x}_{k-1}$ between two consecutive iterations to be smaller or equal to the 15% of $\mathbf{x}_{k-1}$; The third requires all the actual drifts to be smaller than the allowable value with a tolerance of 5%.

Table 1: Values of the parameters used in the numerical examples.

| Parameter | d_{allow} | $\bar{c}_d$ | α | C_l | C_m | C_p | β |
	$[m]$	$[kN\left(\frac{s}{mm}\right)^{\alpha}]$	$[\#]$	$[\#]$	$[1/kN^{0.5}]$	$[\#]$	$[\#]$
Value	0.035	2000	0.35	100	1	50	100

Table 2: Values of the parameters of the continuation scheme of the SLP algorithm.

Parameter	p	s	r	q
Initial value	1.25	0.1	100	100
Increment	1.25 p	1.25 s	20	20
Final value	150	1	∞	∞

In the GA implementation, the population size was set to 350. In order to guarantee the convergence of the algorithm to a global optimum with high probability, 10 different analyses were performed, of which the best solution was chosen. In this case we defined two criteria for convergence: The first halts the algorithm when the number of generations (i.e. iterations) reaches the maximum number allowable `Generations` – 800; The second halts the algorithm when the weighted average relative change in the best fitness function value over `StallGenLimit` generations is less than or equal to `TolFun`. `StallGenLimit` is an integer set to 150, and `TolFun` is a positive scalar set to 10^{-6}.

5.1 Eight-story three bay by three bay asymmetric structure

A 3-D view of the first frame to be optimized is displayed in Figure 3. Based on the results of [57], 16 potential locations for dampers were assigned at the exterior frames in the y direction.
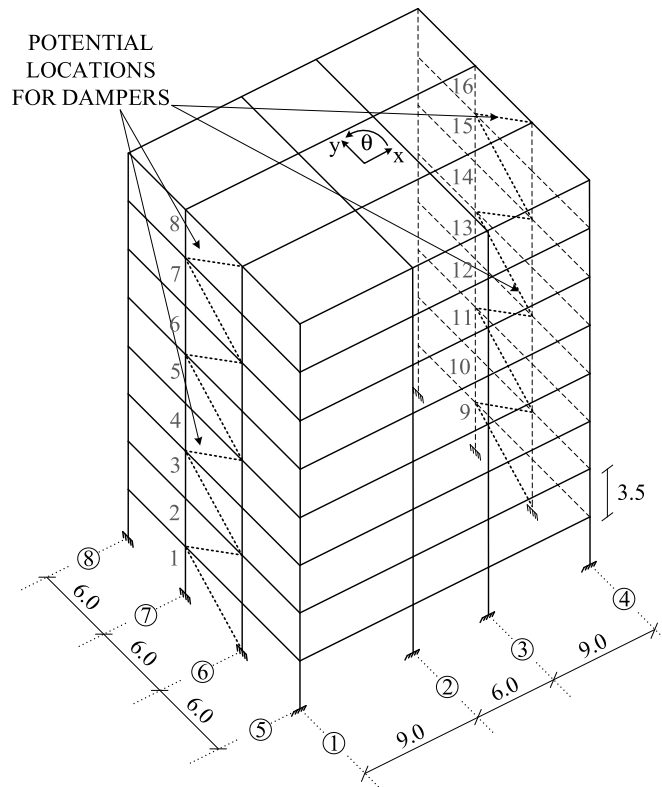

Figure 3: Asymmetric 3-D frame considered in Ex. 5.1.

In the SLP solution, a move limit of 0.05 was considered. The process converged after 91 iterations. The values of the damping coefficients obtained were $\bar{c}_1 = 722.40$ $[kN\left(\frac{s}{mm}\right)^{\alpha}]$ and $\bar{c}_2 = 1178.81$ $[kN\left(\frac{s}{mm}\right)^{\alpha}]$. One slight constraint violation occurred in location number 13 where the drift exceeded the allowable value by 0.32% (i.e. 0.0112 cm). Finally, the optimized solution obtained by the SLP proce-
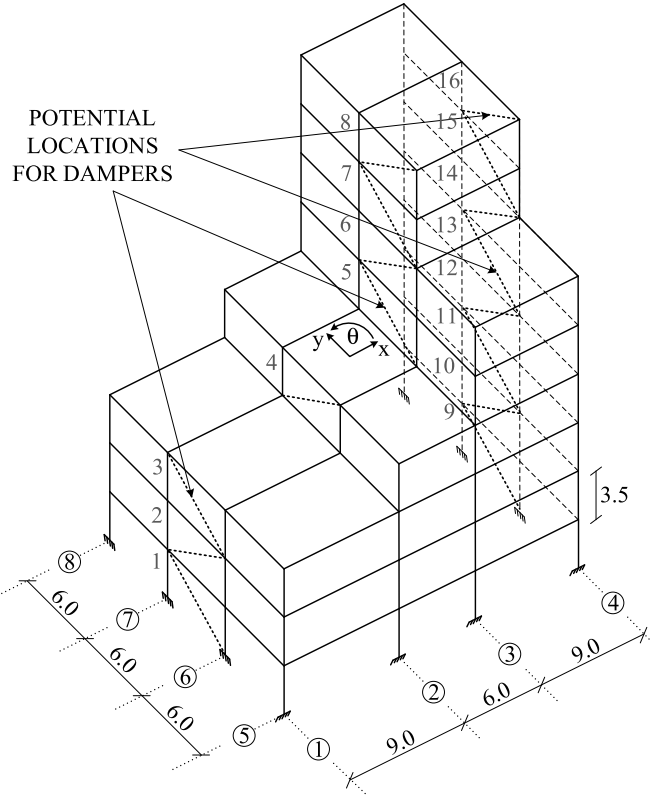
Figure 4: Asymmetric 3-D frame considered in Ex. 5.2.

dure was tested with the other ground motions from the ensemble. None of the other records caused any significant violation of the drift constraint. With GA, the analysis that led to the best solution converged after 199 iterations, leading to the final damping coefficients $\bar{c}_1 = 645.04$ $\left[kN \left(\frac{s}{mm}\right)^{\alpha}\right]$ and $\bar{c}_2 = 995.93$ $\left[kN \left(\frac{s}{mm}\right)^{\alpha}\right]$. The optimized distribution and damper sizes obtained with the two algorithms are shown in Figure 5.
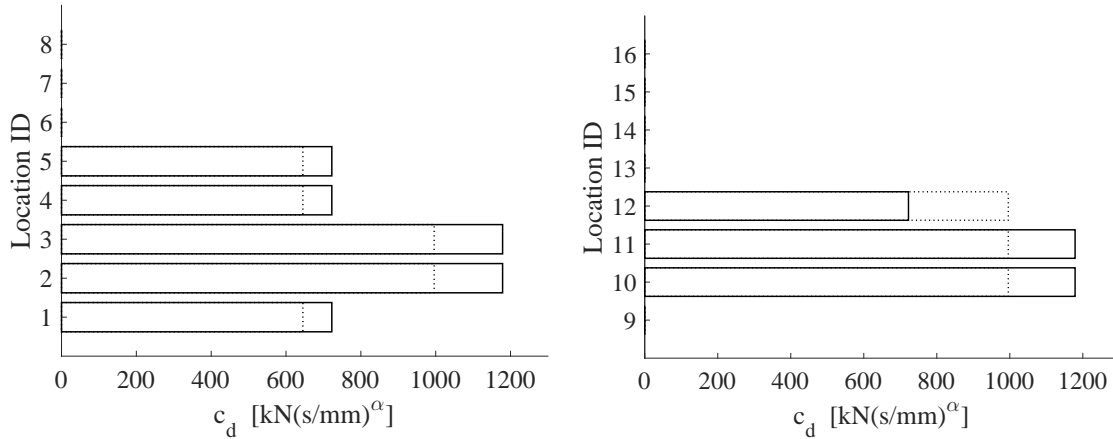

Figure 5: SLP (continuous) and GA (dotted) solutions. Damping coefficient for each location in Ex. 5.1 considering the record $LA16$. The solutions involve dampers of both size-groups in the same locations.

In Table 3 we provide a comparison of the solutions achieved. It is possible to observe that from a numerical point of view the solutions achieved with the two methods are characterized by similar final costs and the same topologies (Figure 5). In fact the two algorithms chose to distribute the dampers in the same locations. The solutions differ in the optimized sizes of the dampers' groups and in the total damping added in each location. This can be justified by the high non-convexity of the problem that causes the presence of several local minima in proximity of the global optima. The main advantage in solving this optimization problem with a gradient based approach is the significant reduction in computational effort

needed to achieve a good solution, compared to that of a GA. To get a satisfying solution with a GA we needed to consider a big population and to repeat several times the optimization analysis. In this case we considered a population of 350 individuals, meaning that the algorithm performed 350 time history analyses in each iteration, and we repeated the optimization process 10 times. On the other hand, the SLP needed to compute two time history analyses each iteration for just one optimization process: one for the structural response and one for the evaluation of the constraint gradient. The final solution of the SLP is also characterized by a small constraint violation, because the SLP solves a series of linear approximations of (28).

Table 3: Comparison of the solutions in Ex. 5.1 considering the record $LA16$. Compared to GA, SLP provides a solution with a similar cost, a small constraint violation, but with a computational effort smaller by 3.58 orders of magnitude.

	$\tilde{J}$, J [#]	$\frac{d_{c,max}}{d_{allow}}$	$\bar{c}_1$ $[kN(\frac{s}{mm})^\alpha]$	$\bar{c}_2$ $[kN(\frac{s}{mm})^\alpha]$	Function evaluations (gradient evaluations are included as function evaluations in the SLP)
SLP	1494.81	1.0032 (0.32%)	722.40	1178.81	$2 \cdot 91 \approx 10^{2.260}$
GA	1471.36	1 (0.00%)	645.04	995.93	$10 \cdot 350 \cdot 199 \approx 10^{5.843}$

In order to further explore the capabilities of the methodology in relation with the cost function we performed another analysis with the SLP and GA considering the same structure, but this time increasing the component of the cost C_p from 50 to 500. As expected, both the algorithms chose a distribution of dampers of a single size-group. The two solutions placed eight dampers in the same locations, slightly differing only in terms of the damping coefficient assigned to the dampers. For a numerical comparison of the results please refer to Table 4.

In particular, with SLP the process converged after 119 iterations. Most importantly, the final designs consisted of only one damper size – as expected due to the high cost related to prototype testing. In fact, eight dampers with damping coefficient $\bar{c}_2 = 1090.60\ [kN\left(\frac{s}{mm}\right)^\alpha]$ were actually placed in locations $1-5$ and $10-12$. The drift in the location number 10 violated the allowable value by the 0.27% (i.e. $0.0095\ cm$). Finally, the optimized design solution was checked with all other records from the ensemble. None of the maximum values of the drifts exceeded significantly the allowable value. With GA, the analysis that led to the best results converged after 173 iterations. As already mentioned, the dampers distribution was almost identical to that of SLP. The final design, in fact, consisted of eight dampers in the same locations as with SLP, and with damping coefficient $\bar{c}_2 = 1096.11\ [kN\left(\frac{s}{mm}\right)^\alpha]$.

Table 4: Comparison of the solutions in Ex. 5.1 with $C_p = 500$, and considering the record $LA16$. Both solutions involves only one size-group of dampers.

	$\tilde{J}$, J [#]	$\frac{d_{c,max}}{d_{allow}}$	$\bar{c}_1$ $[kN(\frac{s}{mm})^\alpha]$	$\bar{c}_2$ $[kN(\frac{s}{mm})^\alpha]$	Function evaluations (gradient evaluations are included as function evaluations in the SLP)
SLP	1943.24	1.0027 (0.27%)	N/A	1090.60	$2 \cdot 119 \approx 10^{2.377}$
GA	1945.39	1 (0.00%)	N/A	1096.11	$10 \cdot 350 \cdot 173 \approx 10^{5.782}$

5.2 Eight-story three bay by three bay double setback structure

In the second example we consider a similar 3-D frame structure but with a double setback. With this example we want to test the ability of the proposed methodology to optimize the added damping system for a structure with a pronounced torsional oscillatory behavior. For a structure of this kind, in fact, we expect the placement of viscous dampers at the peripheries to be a key factor in reducing the inter-story drifts. A 3-D view of the structure is displayed in Figure 4. Also in this case, 16 potential locations for dampers were assigned at the exterior frames in the y direction.

In the SLP procedure the moving limit was relaxed and set to 0.1. This was needed to correct a tendency of the algorithm of getting stuck in unfeasible portions of the design domain during the

initial iterations of the optimization analysis. The optimization process converged after 121 iterations. The optimal design solution was characterized by three dampers with the same damping coefficient $\bar{c}_1 = 1334.70 \ [kN \left(\frac{s}{mm}\right)^{\alpha}]$ placed in locations 1, 9, and 11. The only drift violation occurred in location 10, where the drift exceeded the allowable value by 0.27% (or 0.0095 cm). With GA the analysis that led to the best solution converged after 170 iterations. The algorithm placed dampers in the same locations as the SLP (i.e. locations 1, 9, and 11), assigning to the dampers the same damping coefficient $\bar{c}_2 = 1340.71 \ [kN \left(\frac{s}{mm}\right)^{\alpha}]$.

In this example, the two solutions achieved with SLP and GA were almost identical. However, the computational effort and time required by the SLP was much smaller than that of GA. Looking at the function evaluations in Table 5, it is possible to verify that the ratio between the computational efforts required by the two approaches was approximately 1 : 2500. The GA, in fact, needed to execute 350 nonlinear time-history analyses in each iteration, for 10 different optimization processes. The SLP, on the contrary, performed only two nonlinear analyses in each iteration, as already explained in Sec. 5.1. The solutions achieved with SLP slightly violated the drift constraint because of the linearization adopted for the solution of (28).

Table 5: Comparison of the solutions in Ex. 5.2 considering the record $LA16$. Compared to GA, SLP provides a solution with a similar cost, a small constraint violation, but with a computational effort smaller by 3.39 orders of magnitude.

	$\tilde{J}, J$ [#]	$\frac{d_{c,max}}{d_{allow}}$	$\bar{c}_1$ $[kN(\frac{s}{mm})^{\alpha}]$	$\bar{c}_2$ $[kN(\frac{s}{mm})^{\alpha}]$	Function evaluations (gradient evaluations are included as function evaluations in the SLP)
SLP	607.32	1.0027 (0.27%)	1334.70	N/A	$2 \cdot 121 \approx 10^{2.384}$
GA	608.04	1 (0.00%)	N/A	1340.71	$10 \cdot 350 \cdot 170 \approx 10^{5.775}$

The solution obtained with SLP was tested with the other records from the LA 10% in 50 years ensemble. With two of the records, namely $LA14$ and $LA18$, a significant constraint violation ($> 10\%$) was encountered. Therefore, another optimization analysis was performed, considering simultaneously $LA14$, $LA16$, and $LA18$.

The optimization with SLP converged after 104 iterations. Only dampers with damping coefficient $\bar{c}_2 = 763.62 \ [kN \left(\frac{s}{mm}\right)^{\alpha}]$ were actually placed. The only drift violation occurred in location 12, where the drift exceeded the allowable value by 0.14% (or 0.0049 cm). With GA the analysis that led to the best solution converged after 286 iterations. The values of the damping coefficients obtained were $\bar{c}_1 = 871.60$ $[kN \left(\frac{s}{mm}\right)^{\alpha}]$, and $\bar{c}_2 = 997.67 \ [kN \left(\frac{s}{mm}\right)^{\alpha}]$. The optimized damper size and distribution achieved by the two algorithms are shown in Figure 6.
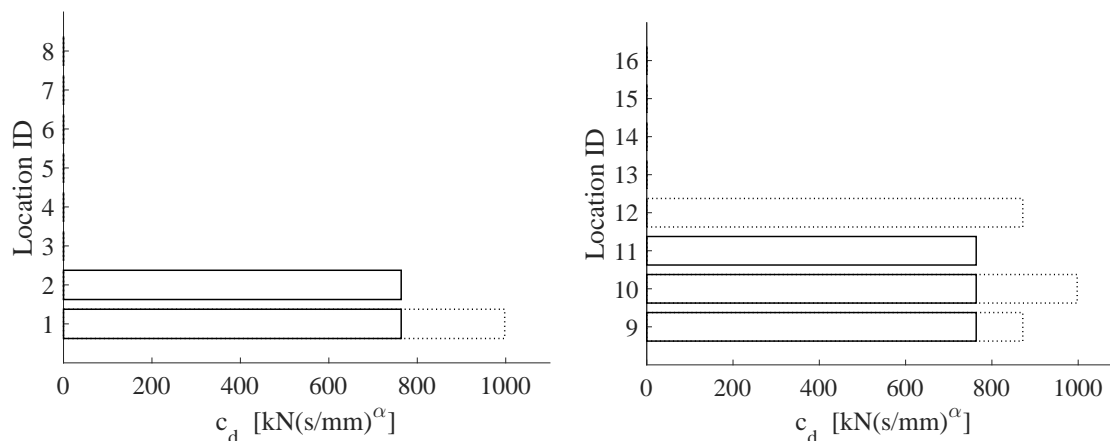

Figure 6: SLP (continuous) and GA (dotted) solutions. Damping coefficients for each location in Ex. 5.2 considering the records $LA14$, $LA16$, and $LA18$. The SLP solution involves dampers of only one size-group.

In this example the solutions achieved with the two approaches were different. The solution obtained

with GA required four dampers only and a smaller final cost, while SLP used one more damper than GA, but involving only one damping (and stiffness) size. Nevertheless, as expected the comparison of the computational effort necessary for achieving the final designs was favorable also in this case for the SLP. In fact, the ratio between the number of function evaluations of the two approaches was approximately $1 : 4800$, for the same reasons given in Sec. 5.1. The difference between the two solutions can be explained by the high nonconvexity of the problem at hand, which causes the presence of several local minima in the surrounding of the global optima. As expected, GA less likely gets influenced by local minima, and in some cases can identify better solutions with respect to those achieved with a gradient-based approach.

Table 6: Comparison of the solutions in Ex. 5.2 considering the records $LA\,14$, $LA\,16$, and $LA\,18$.

	$\tilde{J}$, J [#]	$\frac{d_{c,max}}{d_{allow}}$	$\bar{c}_1$ $[kN(\frac{s}{mm})^\alpha]$	$\bar{c}_2$ $[kN(\frac{s}{mm})^\alpha]$	Function evaluations (gradient evaluations are included as function evaluations in the SLP)
SLP	896.26	1.0014 (0.14%)	N/A	763.62	$6 \cdot 104 \approx 10^{2.795}$
GA	804.33	1 (0.00%)	871.60	997.67	$10 \cdot 350 \cdot 3 \cdot 286 \approx 10^{6.478}$

6 Conclusions

In this paper, we presented a novel approach for the distribution and sizing of nonlinear fluid viscous dampers and their supporting braces based on optimization. A realistic cost function is minimized, considering the economical aspects of the dampers' distribution in a structure, size, and prototype testing. Constrains are imposed on the inter-story drifts at the peripheries of irregular 3-D structures. These are computed with nonlinear time-history analyses considering an ensemble of realistic ground motions. Therefore, the proposed methodology can be used for the performance-based seismic retrofitting of 3-D irregular structures.

The novelty of the proposed approach lies in its formulation which allows a practical minimum-cost design of nonlinear fluid viscous dampers and their supporting members based on optimization. Damper-brace elements are selected from a limited number of available size-groups. The properties of each size-group are also defined by the optimization algorithm. This results in practical design solutions for seismic retrofitting that do not require any additional interpretation. An additional contribution is the reformulation of the original mixed-integer problem into a continuous optimization problem, and the solution with a genetic and a gradient-based algorithm, respectively. The analogy between the two formulations is guaranteed thanks to material interpolation functions, successfully applied in the context of continuum structural topology optimization. All the binary variables of the original mixed-integer formulation are replaced by continuous ones, and their intermediate values are penalized by these interpolation techniques. The resulting penalized continuous formulation implicitly leads the gradient-based algorithm towards a preference of final discrete designs.

The numerical results showed how the proposed methodology successfully solved realistic design cases. In Sec. 5.1 and Sec. 5.2 we showed several examples where both SLP and GA converged to very similar designs. However, if on the one hand the results achieved with the two algorithms were in good agreement in terms of structural performance and cost, on the other hand they also revealed a significant advantage of the gradient-based algorithm in terms of computational effort. This may become even more evident for problems with more design variables, due to the combinatorial nature of the problem, and with more complex governing behaviors for the systems considered (e.g. nonlinear behavior of the structure and of the dampers). The balance between the quality of the final solution and the effort required to achieve it, places gradient-based approaches in an advantageous position over heuristic approaches for practical applications. In many cases, in fact, practitioners dispose of limited computational resources and time for their realistic and complex applications, and it may happen that genetic algorithms are not even a reasonable option. In these cases, we expect the proposed methodology to simplify and promote the optimization-based seismic retrofitting with fluid viscous dampers.

Acknowledgements

References

[1] Taylor D, Duflot P. Fluid viscous dampers used for seismic energy dissipation in structures. *Engineering* 2002; :1–10. (page 1)

[2] McNamara RJ, Taylor DP. Fluid viscous dampers for high-rise buildings. *Structural Design of Tall and Special Buildings* 2003; **12**(2):145–154. (page 1)

[3] Constantinou MC, Symans MD. *Experimental and analytical investigation of seismic response of structures with supplemental fluid viscous dampers.* National Center for Earthquake Engineering Research, 1992. (page 1)

[4] Seleemah AA, Constantinou MC. Investigation of seismic response of buildings with linear and nonlinear fluid viscous dampers. *Technical Report*, University at Buffalo 1997. (page 1, 4)

[5] FIPIndustriale. FIP Industriale web page. URL `www.fipindustriale.it`. (page 2)

[6] TaylorDevices. Taylor Devices Inc. web page. URL `www.taylordevices.com`. (page 2)

[7] Lin WH, Chopra AK. Earthquake response of elastic SDF systems with non-linear fluid viscous dampers. *Earthquake Engineering and Structural Dynamics* 2002; **31**(June 2001):1623–1642. (page 2)

[8] Martinez-Rodrigo M, Romero ML. An optimum retrofit strategy for moment resisting frames with nonlinear viscous dampers for seismic applications. *Engineering Structures* 2003; **25**:913–925. (page 2)

[9] Symans MD, Charney Fa, Whittaker aS, Constantinou MC, Kircher Ca, Johnson MW, McNamara RJ. Energy dissipation systems for seismic applications: current practice and recent developments. *Journal of Structural Engineering* 2008; **134**(1):3–21. (page 2)

[10] Lang ZQ, Guo PF, Takewaki I. Output frequency response function based design of additional nonlinear viscous dampers for vibration control of multi-degree-of-freedom systems. *Journal of Sound and Vibration* 2013; **332**(19):4461–4481. (page 2)

[11] Adachi F, Yoshitomi S, Tsuji M, Takewaki I. Nonlinear optimal oil damper design in seismically controlled multi-story building frame. *Soil Dynamics and Earthquake Engineering* 2013; **44**:1–13. (page 2)

[12] Tubaldi E, Ragni L, Dall'Asta A. Probabilistic seismic response assessment of linear systems equipped with nonlinear viscous dampers. *Earthquake Engineering & Structural Dynamics* jan 2015; **44**(1):101–120. (page 2)

[13] Dong B, Sause R, Ricles JM. Equivalent linearized model of damper response for seismic design of steel structures with nonlinear viscous dampers. *8th International Conference on Behavior of Steel Structures in Seismic Areas*, 2015; 1390–1397. (page 2)

[14] Wang S, Lai Jw, Schoettler MJ, Mahin SA. Seismic Retrofit of a High-Rise Steel Moment Resisting Frame Using Fluid Viscous Dampers. *Improving the Seismic Performance of Existing Buildings and Other Structures 2015*, Dec. 10-12, 2015, American Society of Civil Engineers: Reston, VA, 2015; 121–131. (page 2)

[15] Akcelyan S, Lignos DG, Hikino T, Nakashima M. Evaluation of simplified and state-of-the-art analysis procedures for steel frame buildings equipped with supplemental damping devices based on E-Defense full-scale shake table tests. *Journal of Structural Engineering* 2016; **142**(6):04016 024. (page 2)

[16] Takewaki I, Yoshitomi S. Effects of support stiffnesses on optimal damper placement for a planar building frame. *Journal of the Structural Design of Tall Buildings* 1998; **7**(4):323–336. (page 2)

[17] Singh MP, Verma NP, Moreschi LM. Seismic analysis and design with Maxwell dampers. *Journal of Engineering Mechanics* 2003; **129**(March):273–282, doi:10.1061/(ASCE)0733-9399(2003)129:3(273). (page 2)

[18] Park JH, Kim J, Min KW. Optimal design of added viscoelastic dampers and supporting braces. *Earthquake Engineering and Structural Dynamics* 2004; **33**(4):465–484. (page 2)

[19] Viola E, Guidi F. Influence of the supporting braces on the dynamic control of buildings with added viscous dampers. *Structural Control and Health Monitoring* apr 2009; **16**(3):267–286. (page 2)

[20] Chen YT, Chai YH. Effects of brace stiffness on performance of structures with supplemental Maxwell model-based brace-damper systems. *Earthquake Engineering & Structural Dynamics* jan 2011; **40**(1):75–92. (page 2)

[21] Castaldo P, De Iuliis M. Optimal integrated seismic design of structural and viscoelastic bracing-damper systems. *Earthquake Engineering & Structural Dynamics* 2014; **43**:1809–1827. (page 2)

[22] Lavan O. Optimal design of viscous dampers and their supporting members for the seismic retrofitting of 3D irregular frame structures. *Journal of Structural Engineering* nov 2015; **141**(11):04015 026. (page 2)

[23] Hahn G, Sathiavageeswaran K. Effects of added-damper distribution on the seismic response of buildings. *Computers & Structures* 1992; **43**(5):941–950. (page 2)

[24] Lavan O, Dargush GF. Multi-objective evolutionary seismic design with passive energy dissipation systems. *Journal of Earthquake Engineering* 2009; **13**(April 2014):758–790. (page 2)

[25] Zhang RH, Soong TT. Seismic design of viscoelastic dampers for structural applications. *Journal of Structural Engineering* 1992; **118**(5):1375–1392. (page 2)

[26] Lopez Garcia D, Soong TT. Efficiency of a simple approach to damper allocation in MDOF structures. *Journal of Structural Control* apr 2002; **9**(1):19–30. (page 2)

[27] Agrawal AK, Yang JN. Optimal placement of passive dampers on seismic and wind-excited buildings using combinatorial optimization. *Journal of Composite Materials* 1999; **33**(12):928–940. (page 2)

[28] Dargush GF, Sant RS. Evolutionary aseismic design and retrofit of structures with passive energy dissipation. *Earthquake Engineering and Structural Dynamics* 2005; **34**(May):1601–1626. (page 2)

[29] Kanno Y. Damper placement optimization in a shear building model with discrete design variables: a mixed-integer second-order cone programming approach. *Earthquake Engineering & Structural Dynamics* 2013; **42**(11):1657–1676. (page 2)

[30] Gluck N, Reinhorn AM, Gluck J, Levy R. Design of supplemental dampers for control of structures. *Journal of Structural Engineering* 1996; (DECEMBER):1394–1399. (page 2)

[31] Takewaki I. Optimal damper placement for minimum transfer functions. *Earthquake Engineering & Structural Dynamics* 1997; **26**(February):1113–1124. (page 2)

[32] Takewaki I. Optimal damper placement for planar building frames using transfer functions. *Structural and Multidisciplinary Optimization* 2000; **20**(4):280–287. (page 2)

[33] Singh MP, Moreschi LM. Optimal placement of dampers for passive response control. *Earthquake Engineering and Structural Dynamics* 2002; **31**(April 2001):955–976. (page 2)

[34] Aydin E, Boduroglu MH, Guney D. Optimal damper distribution for seismic rehabilitation of planar building structures. *Engineering Structures* 2007; **29**(2):176–185. (page 2)

[35] Lavan O, Levy R. Optimal design of supplemental viscous dampers for irregular shear-frames in the presence of yielding. *Earthquake Engineering & Structural Dynamics* 2005; **34**(8):889–907. (page 2)

[36] Lavan O, Levy R. Optimal design of supplemental viscous dampers for linear framed structures. *Earthquake Engineering and Structural Dynamics* 2006; **35**(3):337–356. (page 2, 12)

[37] Levy R, Lavan O. Fully stressed design of passive controllers in framed structures for seismic loadings. *Structural and Multidisciplinary Optimization* 2006; **32**(6):485–498. (page 2)

[38] Lavan O, Levy R. Simple Iterative Use of {L}yapunov's Solution for the Linear Optimal Seismic Design of Passive Devices in Framed Buildings. *Journal of Earthquake Engineering* 2009; **13**(5):650–666. (page 2)

[39] Aguirre JJ, Almazán JL, Paul CJ. Optimal control of linear and nonlinear asymmetric structures by means of passive energy dampers. *Earthquake Engineering & Structural Dynamics* 2013; **42**(3):377–395. (page 2)

[40] Lavan O, Amir O. Simultaneous topology and sizing optimization of viscous dampers in seismic retrofitting of 3D irregular frame structures. *Earthquake Engineering and Structural Dynamics* 2014; **43**:1325–1342. (page 2, 3, 7, 9, 13)

[41] Pollini N, Lavan O, Amir O. Towards realistic minimum-cost optimization of viscous fluid dampers for seismic retrofitting. *Bulletin of Earthquake Engineering* 2016; **14**(3):971–998. (page 3, 6, 7, 9, 10, 13)

[42] Taylor D. Personal comunication 2015; . (page 4, 7)

[43] Kasai K, Oohara K. Algorith and Computer Code to Simulate Nonlinear Viscous Dampers. *Passively Controlled Structure Symposium*, Yokohama, Japan, 2001. (page 6)

[44] Oohara K, Kasai K. Time-history analysis model for nonlinear viscous dampers. *Structural Engineers World Congress (SEWC)*, Yokohama, Japan, 2002. (page 6)

[45] Quarteroni A, Sacco R, Saleri F. *Numerical Mathematics, Texts in Applied Mathematics*, vol. 37. Springer Berlin Heidelberg: Berlin, Heidelberg, 2007. (page 6)

[46] Shin H, Singh M. Minimum failure cost-based energy dissipation system designs for buildings in three seismic regions – Part I: Elements of failure cost analysis. *Engineering Structures* 2014; **74**:266–274. (page 6)

[47] Shin H, Singh M. Minimum failure cost-based energy dissipation system designs for buildings in three seismic regions – Part II: Application to viscous dampers. *Engineering Structures* 2014; **74**:275–282. (page 6)

[48] Gidaris I, Taflanidis AA. Performance assessment and optimization of fluid viscous dampers through life-cycle cost criteria and comparison to alternative design approaches. *Bulletin of Earthquake Engineering* 2015; **13**(4):1003–1028. (page 6)

[49] Bendsøe MP, Sigmund O. *Topology Optimization: Theory, Methods and Applications*. Springer, 2003. (page 8)

[50] Eschenauer HA, Olhoff N. Topology Optimization of Continuum Structures: A review*. *Applied Mechanics Reviews* 2001; **54**(4):331–390. (page 8)

[51] Stolpe M, Svanberg K. An alternative interpolation scheme for minimum compliance topology optimization. *Structural and Multidisciplinary Optimization* 2001; **22**:116–124. (page 9)

[52] Sigmund O, Torquato S. Design of materials with extreme thermal expansion using a three-phase topology. *Journal of the Mechanics and Physics of Solids* 1997; **45**(6):1037–1067. (page 9)

[53] Stegmann J, Lund E. Discrete material optimization of general composite shell structures. *International Journal for Numerical Methods in Engineering* 2005; **62**(May 2004):2009–2027. (page 9)

[54] Hvejsel CF, Lund E. Material interpolation schemes for unified topology and multi-material optimization. *Structural and Multidisciplinary Optimization* 2011; **43**(6):811–825. (page 9)

[55] Kanno Y. Global optimization of trusses with constraints on number of different cross-sections: a mixed-integer second-order cone programming approach. *Computational Optimization and Applications* 2016; **63**(1):203–236. (page 9)

[56] Guest JK, Prévost JH, Belytschko T. Achieving minimum length scale in topology optimization using nodal design variables and projection functions. *International Journal for Numerical Methods in Engineering* sep 2004; **61**(2):238–254. (page 10)

[57] Lavan O, Levy R. Optimal peripheral drift control of 3D irregular framed structures using supplemental viscous dampers. *Journal of Earthquake Engineering* 2006; **10**(6):903–923. (page 6, 10, 13, 14)

[58] Cheney EW, Goldstein aa. Newton's method for convex programming and Tchebycheff approximation. *Numerische Mathematik* 1959; **1**(1):253–268. (page 11)

[59] Kelley JE, Kelley Jr JE. The Cutting-Plane Method for Solving Convex Programs. *Journal of the Society for Industrial & Applied Mathematics* 1960; **8**(4):703–712. (page 11)

[60] Michaleris P, Tortorelli Da, Vidal CA. Tangent operators and design sensitivity formulations for transient non-linear coupled problems with applications to elastoplasticity. *International Journal for Numerical Methods in Engineering* jul 1994; **37**(June 1993):2471–2499. (page 11)

[61] Le C, Bruns TE, Tortorelli Da. Material microstructure optimization for linear elastodynamic energy wave management. *Journal of the Mechanics and Physics of Solids* feb 2012; **60**(2):351–378. (page 11)

[62] Jensen JS, Nakshatrala PB, Tortorelli Da. On the consistency of adjoint sensitivity analysis for structural optimization of linear dynamic problems. *Structural and Multidisciplinary Optimization* 2014; **49**(2006):831–837. (page 11)

[63] Hvejsel CF, Lund E, Stolpe M. Optimization strategies for discrete multi-material stiffness optimization. *Structural and Multidisciplinary Optimization* 2011; **44**(2):149–163. (page 12)

[64] Lipp T, Boyd S. Variations and extension of the convex-concave procedure. *Optimization and Engineering* 2016; **17**(2):263–287. (page 12)

[65] Tso WK, Yao S. Seismic Load Distribution in Buildings with Eccentric Setback. *Canadian Journal of Civil Engineering* 1994; **21**(1):50–62. (page 13)

[66] National Information Service for Earthquake Engineering - University of California B. 10 pairs of horizontal ground motions for Los Angeles with a probability of exceedence of 10% in 50 years. (page 13)